Risk Patterns and Correlated Brain Activities. Multidimensional statistical analysis of fMRI data with application to risk patterns

Alena Myšičková[a,**], Song Song[b], Piotr Majer[b], Peter N.C.Mohr[c], Hauke R. Heekeren[c], Wolfgang K. Härdle[b]

[a] *Max Planck Institute for Molecular Genetics, Berlin*
[b] *C.A.S.E. Center for Applied Statistics and Economics, Humboldt-Universität zu Berlin, Berlin*
[c] *Max Planck Institute for Human Development, Berlin Freie Universität Berlin*

Abstract

Decision making usually involves uncertainty and risk. Understanding which part of the human brain is activated during risky decisions and whether there is a significant response to specific stimuli in the hemodynamic response (neural processes underlying investment decisions) are important goals in decision neuroscience. We apply an investment decision task on 17 subjects exercised in the functional magnetic resonance imaging (fMRI) scan. We obtain a time series of three-dimensional images of the blood-oxygen-level dependent (BOLD) fMRI signals. The challenge is to capture the dynamic behavior of specific brain regions in this high-dimensional time series data, by a flexible factor approach resulting in a low dimensional representation. We reanalyze this data from a previously published study Mohr et al. (2010) by applying the panel version of the dynamic semiparametric factor model (DSFM) presented in Park et al. (2009), which can identify the corresponding activations in space and dynamics in time. Further, we classify the risk attitudes of all subjects based on the estimated low-dimensional time series. Our classification analysis confirm the estimated risk attitudes derived from subjects' decision behavior directly.

*The authors greatfully acknowledge financial support from the Deutsche Forschungsgemeinschaft through SFB 649 "Economic Risk".

**Corresponding author
Email address: mysickov@molgen.mpg.de (Alena Myšičková)

Keywords: risk, risk attitude, fMRI, decision making, medial orbifrontal cortex, semiparametric model, factor structure, SVM
JEL classification: D8, C14, C3

1. Introduction

Decision making is a complex process of integrating and comparing various aspects of choice options. In the past years decision neuroscience has made important progress in grounding these aspects of decision making in neural systems (Heekeren et al., 2008; Rangel et al., 2008). Several different models describe decision making as a process consisting of two sub-processes: valuation and comparison. Individuals are assumed to first evaluate the different choice alternatives, then compare the different values, and finally choose the one with the highest value. Expected Utility Theory (EUT)(von Neumann and Morgenstern, 1953), Prospect Theory (Kahneman and Tversky, 1979), and the Mean-Variance Model (Markowitz, 1952) are important examples for value-based decision models. Decision neuroscience has frequently investigated neural representations of value, the crucial metric in value-based decision models. One study investigated the value of monetary rewards during intertemporal choice (Kable and Glimcher, 2007). In this study, the subjective value of delayed monetary rewards was modeled with a hyperbolic function and was significantly correlated with the blood oxygen level dependent (BOLD) response in the ventromedial prefrontal cortex (VMPFC), posterior cingulate cortex (PCC), and ventral striatum (VST). Another study investigated the value of food products in a consumer choice paradigm (Plassmann et al., 2007). Determined by the willingness-to-pay, the subjective value of the food products correlated with the BOLD signal in the medial orbitofrontal cortex (mOFC) and the dorsolateral prefrontal cortex (DLPFC). These and other studies indicate that the value of a choice alternative is represented in a network consisting of mOFC/VMPFC, VST, and PCC. Although most models of decision making share the idea of a value metric that is determined and compared to make a decision, the assumed valuation process differs significantly from one model to another.

For decisions under risk a crucial metric that is assumed to influence the value of a choice alternative is the decision maker's risk attitude. In utility-based models of decision making under risk (e.g., EUT) the risk attitude determines the curvature of the utility function, thereby influencing the valuation process of risky choice alternatives. Risk-return models (Sarin and

Weber, 1993; Weber and Johnson, 2009b), in contrast, incorporate the risk attitude as a weighting factor on the risk metric of the model. So far only a few studies tried to identify neural representations of risk attitude or neural mechanisms reflecting the effect of the risk attitude on the valuation process. One study found correlations between risk attitude and risk-related brain activity in lateral OFC for risk averse individuals and in mOFC for risk seeking individuals (Tobler et al., 2007). Another study found that inter-individual differences in decision-related brain activity in lOFC and PCC correlated with inter-individual differences in risk attitudes independent of the current level of risk (Mohr et al., 2010). Finally, the authors of a latter study could show that the value signal in the VLPFC increased with risk in risk seeking individuals and decreased with risk in risk averse individuals, thereby reflecting the risk attitude.

All of the above mentioned studies applied a generalized linear model (GLM) to analyze the fMRI data. Although it is frequently used in neuroscience and has led to important insights into the neurobiological processes underlying cognition and emotion, the GLM approach has some important limitations. First, it focuses on task-related changes in the mean BOLD signal. Thereby, the GLM neglects information that might be carried by the variability of the BOLD signal (Mohr and Nagel, 2010). For example, a recent study found that the relationship between age and the number of risk-seeking mistakes in a risky decision making task was mediated by the temporal variability of the BOLD signal (Samanez-Larkin et al., 2010). Further, the GLM is a model-based approach to analyze fMRI data, and can therefore only detect effects that were previously hypothesized and modeled. Recent advances in model-free analysis techniques, such as the tensor probabilistic independent component analysis (T-PICA) (Beckmann and Smith, 2005), in contrast, have the potential to detect effects without any constraints on a priori hypotheses and/or modeling.

In line with these approaches we investigated individual differences in risk attitudes with a model-free analysis technique, setting a special focus on the temporal variability of its components. Specifically, we used the dynamic semiparametric factor model (DSFM) introduced by Park et al. (2009) to reduce dimensions of the high-frequent, high-dimensional multisubject fMRI data. DSFM estimates both spatial factors common for all studied subjects and subject-specific factor loadings in temporal domain. In other words, it provides joint spatial factors and combines the temporal and subject domain in the subject-specific time-series loadings. Therefore DSFM factorisation

techniqe is similar to T-PICA approach (Beckmann and Smith, 2005). However, in the latter the full data set is decomposed into factors in all three domians (spatial, temporal and subject). Compared to DSFM this leads to greater number of model control variables to be fixed and parameters to be estimated. The parsimoniousness and flexibility of DSFM allows us to capture the variability of corresponding brain regions by subject-specific time-series loadings. Finally, we hypothesize that the temporal variability of components corresponding to high loadings in brain regions related to value processing (e.g. mOFC/VMPFC, VST, and VLPFC) is related to the risk attitudes of individuals.

2. Materials and Methods

Experimental procedures

We reanalyzed data from a previously published study Mohr et al. (2010). 22 young volunteers (age 18−35 years, 11 females) participated in this study. All participants were native German speakers, right-handed and had no history of neurological or psychiatric diseases. Three participants had to be excluded due to extensive head motion ($>$ 5 mm absolute head movement) modeling problems (always chose the risky alternative). Next two were excluded due to different scanning frequency.

Each trial of the Risk Perception and Investment Decision (RPID) task consisted of two phases: the presentation of a return stream, followed by a decision or subjective judgment task (see Fig.1). In investment situations investors are often confronted with past performance data of possible investments. To mimic this situation, in the first phase we sequentially presented a stream of 10 returns from an investment, each presented for 2 s without fixation-phases between the returns. These 10 returns provided information about the past performance of a given investment. In the experiment, each return stream was independent of the others and described a new investment option. We varied the mean and the standard deviation of the return streams parametrically with three means (6%, 9%, and 12%) and three standard deviations (1%, 5%, and 9%), resulting in nine different combinations of means and standard deviations. In the second phase, subjects performed one of three possible tasks in each trial (each 7 s) without knowing in advance which one they would have to perform after the stream.

We used three tasks to be able to investigate choices as well as perceived risk and subjective expected return, as specified in recent psychological risk-

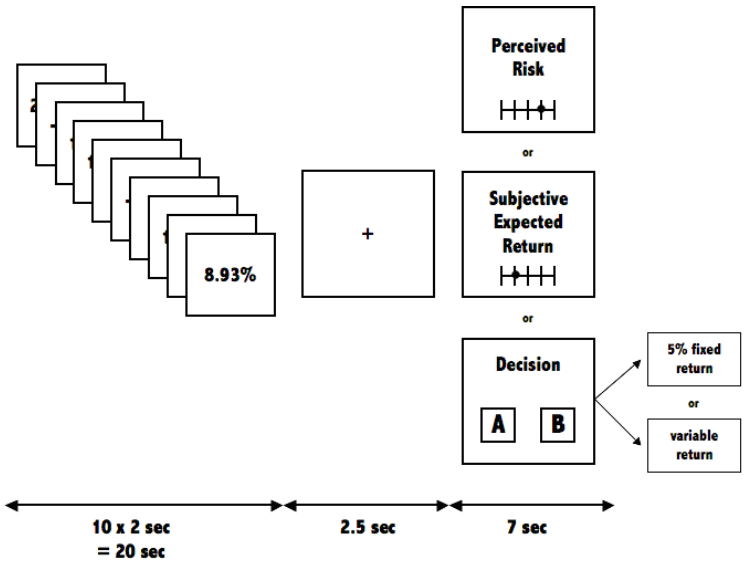

Figure 1: RPID task: Subjects were presented with streams of 10 returns from an investment. Then, they either (a) judged the subjective expected return of the return stream, (b) judged the perceived risk of the return stream, or (c) chose between an investment with a fixed return of 5% and an investment with a variable return which was represented by the return stream.

return models (Weber and Johnson (2009a)). In the decision task the subjects had to make a choice between an investment with 5% fixed return (safe investment) and the investment represented by the return stream they just saw (risky investment). In the other two tasks subjects reported their subjective expected return and perceived risk of the investment represented by the return stream. Subjects indicated subjective expected return on a scale ranging from -5% to +15% and perceived risk on a scale ranging from 0 (no risk) to 100 (maximum risk) (Klos et al. (2005)). Subjects performed each task (decision, subjective expected return, perceived risk) 27 times (81 trials in total). Before the experiment subjects completed four training trials, knowing that the standard deviations in the experiment would be in the same range as in the training trials. No explicit information regarding means or standard deviations was given to the participants. Subjects received a flat payment of 10 Euro for their participation in the experiment and a virtual endowment of 100 Euros to invest. They were explicitly told that the returns they observe during the experiment are randomly drawn from Gaussian dis-

tributions. They were further instructed that after the experiment, 1 of their 27 choices will be randomly chosen to determine decision dependent payments. If the subject would choose the safe option in the respective trial, she would get 5 Euros (5% of 100 Euros) in addition to the 10 Euros. If a subject would choose the risky option in this trial, a random return was drawn from a Gaussian distribution with the same mean and standard deviation as the respective return stream. The resulting outcome (return times 100 Euro) was added to or subtracted from the flat payment.

Behavioral Modeling

According to subjects' responses a risk attitude for each individual could be estimated. We applied the following psychological risk-return model (detailed description can be found in Mohr et al. (2010)):

$$V(x) = \mu(x) - \phi\sigma(x) \tag{1}$$

In this equation $V(x)$ defines the *value* a subject assigns to an investment x, $\mu(x)$ represents the *subjective expected return*, $\sigma(x)$ represents the *perceived risk*, and ϕ is the individual risk weight.

To determine which model predicted *subjective expected return* and *perceived risk* judgments best, we used a "leaving one out at a time" cross-validation method, which ensures the predictive power especially in situations with few trials. First, we divided trials into 26 fitting trials and one test trial. Second, we estimated the parameters for every model that maximized the correlation between model predictions and stated *subjective expected returns* and *perceived risks*. For *subjective expected return* we compared five different models: (1) *mean*, (2) *recency*, (3) *primacy*, (4) *overweight* $< 0\%$, and (5) *overweight* $< 5\%$. All models are weighted average models that we modeled with memory (number of returns over which the model was computed) and weighting as free parameters. Regarding *perceived risk* we compared six different models: (1) *standard deviation*, (2) *coefficient of variation*, (3) *probability* $< 0\%$, (4) *probability* $< 5\%$, (5) *range*, and (6) *coefficient of range*. Whereas the *standard deviation* and the *range* are measures of variation, the *coefficients of variation* and *range* are measures of variation divided by the mean. *Probability* $< 0\%$ and *probability* $< 5\%$ are models for the probability of a loss given a particular loss threshold. The only free parameter in all models was memory (number of returns over which the model was computed). Model predictions of risk models, generated by applying the models

on the return streams, were regressed on the stated perceived risks to allow a transformation of the model predictions (which depend on the scale of the returns) into the dimensions of the scale used in the experiment (0–100).

Third, we applied all models to the return stream of the test trials, making predictions for subjective expected return and perceived risk. We then calculated the squared difference between model predictions and stated subjective expected returns/perceived risks in the test trial. We repeated this procedure for all 27 trials, that is, each trial once served as the test trial. The models with the least average squared difference between model predictions and stated subjective expected returns/perceived risks were identified as individual best models for subjective expected return and perceived risk. Finally, we used all 27 trials to estimate the parameters of these best models, which were later used to predict subjective expected return and perceived risk during choice trials.

We used these predictions to estimate the risk weight and test the risk-return models behaviorally. Risk weights were estimated by fitting a softmax function to the choice data. Best risk weights maximized the sum of loglikelihoods of all 27 choices. Additionally, we tested how many of the actual choices could be explained by the fitted risk weight, if we assume a deterministic decision rule. The decision rule was defined as follows. If $V(safe) > V(risky)$ the individual chooses the safe option and vice versa. The *value* of the safe option is always constant ($V(safe) = 5\% - \phi \cdot 0 = 5\%$) because there is no risk involved. This risk weight was then used to make a prediction about the choice in all 27 trials. To compare the psychological risk-return model with the normative risk-return model we repeated the above described procedures for this model.

The risk attitude can be measured as value reduction in Euro for maximum risk (the case when the subjective perceived risk = 100), as described in Mohr et al. (2010). All subjects were classified as risk averse indicated by a positive risk weight. However, for seven subjects the risk attitude was low (risk weight ≤ 5) resulting in only a small influence of risk on value. For that purpose the seven subjects with the lowest risk attitude were classified as weakly risk-averse. All subjects with risk weight > 5 were classified as strongly risk-averse.

fMRI data acquisition

fMRI data were acquired on a 1.5 T Magnetom Sonata fMRI system

(Siemens, Erlangen, Germany) equipped with a standard head coil. We used a vacuum pad to minimize head motion. Functional images were acquired using a BOLD-sensitive T2*-weighted echo-planar imaging (EPI) sequence [TR, 2500 ms; echo time (TE), 40 ms; flip angle, 90; field of view, 256 mm; matrix, 64 x 64 mm; 26 axial slices approximately parallel to the bicommissural plane; slice thickness, 4 mm]. Two functional runs were acquired (735 and 625 volumes). The first two scans of each run were discarded to allow longitudinal magnetization to reach equilibrium. After the functional runs, a high-resolution structural image was acquired to aid in normalization and co-registration.

fMRI data analysis

Due to the computational limitations (software memory capacity), we used the first part (first 722 observations of 735 that include all 45 trials) of the experiment for our analysis. The data was initially pre-processed with FSL 4.0 (FMRIB's Software Library, http://www.fmrib.ox.ac.uk/fsl/). Pre-processing included motion correction and slice-time correction. Additionally, images were normalized into a standard stereotaxic space (Montreal Neurological Institute (MNI), Montreal, Quebec, Canada).

To capture the temporal variability in the high-dimensional fMRI series, that may be related to individual differences in risk attitude, here we used a dynamic semiparametric factor model (DSFM) which was proposed by Park et al. (2009). DSFM is a model-free multivariate method, which is able to identify activated brain regions (factors) and corresponding low dimensional time series (factor loadings) in only one estimation step Park et al. (2009). In addition, the panel version of the DSFM allows determining active brain areas for multiple subjects, whereas the individual changes are described by subject-specific time series.

From a statistical point of view the BOLD signal of all voxels during the whole experiment can be considered as a multi-dimensional time series. The following DSFM is calibrated to study such high-dimensional time series:

$$\begin{aligned} Y_{t,j} &= m_0(X_{t,j}) + \sum_{l=1}^{L} Z_{t,l}\, m_l(X_{t,j}) + \varepsilon_{t,j}, \;\; 1 \le j \le J,\; 1 \le t \le T. \\ &\stackrel{\text{def}}{=} Z_t^\top m(X_{t,j}) + \varepsilon_{t,j} = Z_t^\top A^* \Psi_{t,j} + \varepsilon_{t,j}\ . \end{aligned} \tag{2}$$

Here, $Z_t = (\mathbf{1}, Z_{t,1}, \ldots, Z_{t,L})^\top$ is an unobservable L-dimensional stochastic process and m is an L-tuple $(m_1, \ldots, m_L)$ of unknown real-valued functions m_l. $X_{t,j} \in \mathbb{R}^d$ are known predictors and $Y_{t,j} \in \mathbb{R}$ is the response variable of interest (the BOLD signal). The errors $\varepsilon_{t,j}$ are assumed to have zero means and finite second moments. The functions m_l are approximated by a space basis $\Psi_{t,j} = [\psi_1(X_{t,j}), \ldots, \psi_K(X_{t,j})]^\top$ and corresponding $(L+1) \times K$ matrix of unknown coefficients A^*. More precisely, $[\psi_1(X_{t,j}), \ldots, \psi_K(X_{t,j})]^\top$ denote quadratic tensor B-splines on K equidistant knots. The estimates of $Z_t^\top$ and A^* are found by minimizing:

$$S(\widehat{Z}_t, \widehat{A^*}) = \arg\min_{Z_t, A^*} \sum_{t=1}^{T} \sum_{j=1}^{J} \{Y_{t,j} - Z_t A^* \Psi_{t,j}\}^2 \tag{3}$$

The minimum is found by the Newton-Raphson algorithm. The parametric part $\widehat{Z}_t$ captures the evolution in time, while $\widehat{A^*}$ represents the smooth, nonparametrically estimated spatial structure.

In our experiment, the voxel's index (i_1, i_2, i_3) is the covariate $X_{t,j}$ and the normalized BOLD signal the dependent variable $Y_{t,j}$; $j = 1, \ldots, J$; $t = 1, \ldots, T$. To simplify numerical operations blank areas were removed from the original data. Thus, the spatial and temporal dimensions equals $J = 91 \times 92 \times 71 = 594\,412$ and $T = 722$, respectively. Such that the covariate is time-invariant and it follows: $X_{t,j} = X_j = (i_1, i_2, i_3) \in \{(1; 91), (1; 92), (1; 71)\}$.

To analyze all tested subjects $i, i = 1, \ldots, I$ in one model, we extended (2) to a panel dynamic semiparametric factor model (PDSFM):

$$Y_{t,j}^i = m_0(X_j) + \sum_{l=1}^{L} \left(\overline{Z}_{t,l} + \alpha_{t,l}^i\right)\ m_l(X_j) + \varepsilon_{t,j}^i,$$
$$1 \le j \le J,\ 1 \le t \le T,\ 1 \le i \le I\ .$$

$\alpha_{t,l}^i$ is the fixed individual effect for subject i on function m_l at time point t. For identification purpose, we assume that the individual effects over all subjects and over all functions m_l sums to zero, e.g.:

$$\mathrm{E}\left[\sum_{i=1}^{I}\left(\sum_{l=1}^{L} \alpha_{t,l}^i m_l(X_j) | X_j\right)\right] = 0. \tag{4}$$

It is reasonable to claim that different subjects have different patterns of brain activation (to the external stimuli and characterized by different stochastic processes Z_t^i), but they share essentially the same spatial structure of the brain (characterized by the same m_l functions). Our analysis concentrates on the detection of those common active brain regions over all subjects. Hereinafter, we assume that these regions are homogeneous for all individuals and therefore can be modeled by a joint (average) spatial factors denoted as $\overline{m}_l,\ l = 1, \ldots, L$. The activation differences between the individuals are captured by their specific low-dimensional time series $Z_{t,l}^i$.

For the averaged fMRI series $\overline{Y}_{t,j}$ holds an equivalent relation to (2):

$$\overline{Y}_{t,j} = \overline{m}_0(X_j) + \sum_{l=1}^{L} \overline{Z}_{t,l}\overline{m}_l(X_j) + \varepsilon_{t,j}\ ,\quad 1 \le j \le J\ ,\ 1 \le t \le T\ , \tag{5}$$

with factor loadings $\overline{Z}_{t,l}$ corresponding to common factors $\overline{m}_l$.

After the spatial functions are determined, the subject specific time series $\widehat{Z}_{t,l}^i$ can be estimated using the ordinary least square method:

$$Y_{t,j}^i = \overline{m}_0(X_j) + \sum_{l=1}^{L} Z_{t,l}^i \overline{m}_l(X_j) + \varepsilon_{t,j}^i\ . \tag{6}$$

The statistical inference of the whole system is then based on the low-dimensional time series analysis. Park et al. (2009) has shown that the difference between the inference based on the estimated low-dimensional time series and the "true" unobserved time series is asymptotically negligible.

Our multi-subject multivariate estimation procedure can be summarized in the following steps:

1. Take the average $\overline{Y}_{t,j}$ of $Y_{t,j}^i$ across all subjects $i \in \{1, 2, \ldots, I\}$ and estimate the common spatial factors $\widehat{\overline{m}}_l(X_j)$, as in the original DSFM approach (2).
2. Given the common $\overline{m}_l(X_j)$ estimate the subject-specific temporal factor loadings $\widehat{Z}_{t,l}^i$ from (6). Repeat this estimation procedure for all $i = 1, \ldots, I$.
3. Analyze the joint factors $\overline{m}_l(X_j)$, significant active brain regions are defined by the threshold of 0.5%- and 99.5%-quantiles of the empirical distribution function of $\overline{m}_l(X_j)$ in all voxels.

4. Find the variations between individuals by looking at the factor loadings $\widehat{Z}^i_{t,l}$. Is it possible to reconstruct subjects' behaviour just by analyzing this low-dimensional time series?

3. Results

In this section we describe the choice of the model parameters for the studied data set. Further, we describe a selection of estimated factors and corresponding factor loadings. The classification procedure described in the last paragraph is based only on the fMRI data and predicts the subjects' risk aversion with a high precision.

Model parameters

The analysed raw data are high-dimensional ($722 \times 594\ 412 = 429\ 165\ 464$). We have chosen quadratic tensor B-splines on equidistant knots as the space basis Ψ_j. The numbers of knots in the three directions were set to $12, 14, 14$, respectively, which is a trade-off between the best possible resolution and a reasonable computational time. With this parameter choice, $250 = (91 \times 92 \times 71)/(14 \times 14 \times 12)$ points correspond to one 3 dimensional quadratic B-spline basis function.

The most important parameter in our model is the number of factors (and corresponding factor loadings) L. The choice of L was based on both, the specificity of factors interpretation m_l, $l = 1, \ldots, L$ and the averaged explained variance by factors:

$$EV(L) = 1 - \frac{\sum_{t=1}^{T} \sum_{j=1}^{J} \left\{ Y_{t,j} - \sum_{l=0}^{L} Z_{t,l} m_l(X_{t,j}) \right\}^2}{\sum_{t=1}^{T} \sum_{j=1}^{J} \left\{ Y_{t,j} - \bar{Y} \right\}^2} .$$

Table 1: Explained variation in percent of the model with different numbers of factors L. The explained variation is averaged over all 17 analyzed subjects.

$L = 2$	$L = 4$	$L = 5$	$L = 10$	$L = 20$
92.07	92.25	92.29	93.66	95.19

Table 1 shows the averaged explained variation for different numbers of factors. Here, only slight differences between the explained variation for

$L \geq 2$ can be observed. The fMRI signals $Y_{t,j}$ were explained mostly by the null-factor and the first 2 factors: $\widehat{m}_0(X_{t,j}) + Z_{t,1}\widehat{m}_1(X_{t,j}) + Z_{t,2}\widehat{m}_2(X_{t,j})$. The relatively small effects of the functions m_l for $l \geq 2$ are due to the small differences of activation in the selected regions. The inclusion of greater number of factors leads to detection of the important areas for decision making under risk. We choose $L = 20$, which allows for relatively low complexity and an explicit interpretation of the functions $\widehat{\widehat{m}}_l$. Residual analysis, as shown in Appendix B, supports our model selection.

Factors $\widehat{m}_l$

In our study we were looking for spatial maps which undergo significant changes in BOLD signal during the experiment. Those spatial maps(factors) determine the regions while the time evolution and subject specificity are captured by the corresponding factor loadings $Z^i_{t,l}$. After applying the DSFM technique we estimated 20 spatial factors. 6 of them ($\widehat{m}_l$, $l = 5, 9, 12, 16, 17, 18$) correspond to brain areas which were already found in decision making contexts (e.g. Heekeren et al. (2008), Rangel et al. (2008), for review) : mFOC and Parietal Cortex (Fig. 2). Only voxels with the highest values $\widehat{m}_l(X_j) \geq 99.95\%$ of the empirical quantile are shown. Factors $\widehat{m}_5$, $\widehat{m}_9$, $\widehat{m}_{16}$, $\widehat{m}_{17}$ and $\widehat{m}_{18}$ have the largest values in the medial orbitofrontal cortex (mOFC), located in the bottom frontal part of the brain (Fig. 2). mOFC is associated with the value of a choice option Plassmann et al. (2007). Factor $\widehat{m}_9$ represents the Parietal Cortex. Beside these interesting factors connected with decision making, , we detected other spatial maps that correspond to motor and visual areas, likely unrelated to the decision making process within the task.

Herewith, we have shown, that the estimated function $\widehat{m}_l$, $l = 1, \ldots, L$ in our model represent those brain regions which were expected to be involved during the experiment (visualisation, motoric and value-of-choice areas). The activity of these regions changes both over the subjects and over the experiment. This variability is described by the factor loadings $Z^i_{t,l}$ for $t = 1, 2, \ldots, T$ $l = 1, 2, \ldots, L$ $i = 1, \ldots, I$ which are discussed in the next session.

Factor loadings $\widehat{Z}_{t,l}$

The dynamics and subject specificity are jointly represented by the low-dimensional time series $\widehat{Z}^i_t$. These subject-specific $\widehat{Z}^i_{t,l}$ correspond to the individual temporal differences of the activated brain regions in $\widehat{m}_l$. For

better illustration we have selected the two extreme subjects (see the estimated factor loadings $\widehat{Z}_{t,12}$ and $\widehat{Z}_{t,18}$ in Fig.3). Both time series show a high fluctuation around their mean value.

To get a better insight into the dynamics of the time series, a detailed view of $\widehat{Z}_{t,12}$ of subject 12 in 200 (out of 722) data points with highlighted 3 different types of stimulus (e.g. decision, subjective expected return, perceived risk) is shown in Fig. 4. The most important values of the factor loading $Z_{t,l}$ are the next 3 observation after stimulus, which are measured up to a maximum of 7.5 seconds after stimulus, as the hemodynamic response has its peak usually around 6 seconds after the stimulus onset. Figure 5 shows these responses for studied factor loadings and representative subjects. Formally, we plotted $\Delta\widehat{Z}_{t,l} \stackrel{\text{def}}{=} \widehat{Z}_{s+t,l} - \widehat{Z}_{s,l}$ against t, where s is the time when a stimulus was given. In Figure 5, one can observe that the responses to the stimulus of the most extreme of the weakly risk-averse individuals show a significantly different volatility than the responses of the most extreme of the strongly risk averse individuals. . We found this volatility pattern in all factor loadings corresponding to the selected factors ($l = 5, 9, 12, 16, 17, 18$).

Risk classification

After we could reasonably interpret the estimated factors $\widehat{\overline{m}}_l$ and described the behavior of the factor loadings $\widehat{Z}^i_{t,l}$ we tried to connect our findings with the risk attitude of the subjects. Without knowing the subjects' answers, based only on low-dimensional $\widehat{Z}^i_{t,l}$ representation of BOLD signal, we develop a classification method which can predict the risk attitude. For this purpose we use the functions $\Delta\widehat{Z}^i_{t,l}$, $l = 5, 9, 12, 16, 17, 18$ and $i = 1, 2, \ldots, I$ since they correspond to the brain activity of factors, which are linked with utility and decisions under risk. In the classification analysis, only the 3 observation points after the stimulus were taken into account (see paragraph *Factor loadings* $\widehat{Z}_{t,l}$).

As described in Section 2, there were 3 different types of answers which subjects had to make. According to this, we considered $\Delta\widehat{Z}^i_{t,l}, l = 5, 9, 12, 16, 17, 18$ only after the decision onset. To capture the variability in the stimulus responses (since the observations are not exactly in time points of the BOLD peak), we calculated the average value of the responses after each of the 15 decision exercise: $\overline{\Delta}\widehat{Z}^i_{s,l} = \frac{1}{3}\sum_{\tau=1}^{3}\Delta\widehat{Z}^i_{s+\tau,l},\ l = 5, 9, 12, 16, 17, 18$. Here, $\overline{\Delta}\widehat{Z}^i_{s,l}$ denotes the average reaction to the decision stimulus after the task s, for loading l and subject i. Further, we calculated the variance of $\overline{\Delta}\widehat{Z}^i_{s,l}$ and

observed higher variability for weakly risk averse subjects than for strongly averse (see Appendix A). In order to confirm that finding, these 6 variables, corresponding to $l = 5, 9, 12, 16, 17, 18$, were chosen as the input variables for the classification algorithm.

In the next step, we classify studied subjects according to their risk attitude based on data extracted from the BOLD signal only (without knowing the subject's estimated risk attitude). Classification analysis of the subjects was conducted via Support Vector Machines (SVM), a widely used nonlinear method based on statistical learning theory of Cortes and Vapnik (2005). In the learning step, strongly risk averse subjects were labeled with 1 and the weakly risk averse subjects with -1. The estimated risk attitude described in *Behavioral Modeling* were used for the validation of the classification predictions. In order to avoid overparametrization and too optimistic results we applied the double cross-validation method to tune the SVM and estimate the classification rate. The algorithm can be described as follows

1. separate the data into training set and testing set (leave-one-out procedure)
2. apply the leave-one-out cross validation on the training set only and tune the algorithm
3. classify the testing data
4. repeat 1-3 for all different testing sets
5. average the classification rate over all iterations 4.

Using the standard deviation of the differences and the optimal SVM parameters, the classification rate was optimal (100%) for strongly risk averse and 85.71% for weakly risk averse individuals (Table 2). We compare our classification performance with an SVM classifier taking as input variables the mean of the averaged reaction to the decision stimulus $\overline{\Delta}\widehat{Z}_{t,l}$. Table 2 clearly shows that the mean of the averaged reaction does not indicate any differences between weakly and strongly risk averse subjects. Yet, these 2 classes can be distinctly identified by their volatility. The risk attitude of the subject is derived directly from the time series $\widehat{Z}^i_{t,l}$, $l = 5, 9, 12, 16, 17, 18$; - the low-dimensional representation of the BOLD signals series.

We have provided the SVM classification using a wide range of prior parameters to the Gaussian kernel, the capacity C and the radial basis coefficient r. Table 3 summarizes the results obtained by using different values of these parameters. The classification rates are the averages over the parameter range.

Table 2: Classification rates of the SVM method using standard deviation (left) and mean (right) of the $\Delta\widehat{Z}_{t,j}, j = 5, 9, 12, 16, 17, 18$.

STD		Estimated		MEAN		Estimated	
		Strongly	Weakly			Strongly	Weakly
Data	Strongly	1.00	0.00	Data	Strongly	0.70	0.30
	Weakly	0.14	0.86		Weakly	0.55	0.45

Table 3: Classification rates of the SVM method using different values of parameters r and C for mean and standard deviation.

	Rate	r	C
Std	0.81	$0.6 - 1.00$	$1 - 80$
Mean	0.60	$0.02 - 1.00$	$1 - 80$

4. Discussion

Decision making is a complex process consisting of valuation, comparison and the final choice. Decision neuroscience has frequently investigated neural representations of value, the key metric in the decision models. Previous studies showed that the BOLD response in VMPFC, PCC, VST, mOFC and DLPFC are activated during the valuation process. For decisions under risk, risk attitude is the crucial metric that is assumed to influence the value of a choice alternative. Up to now, only few studies tried to identify neural representations of risk attitude, correlated regions were found in lOFC, mOFC, PCC and VLPFC.

The usual technique used in neural studies to evaluate the fMRI data is the GLM approach. This approach has some limitations which are crucial for the identification of brain regions associated with risk attitude. GLM focuses on the changes in the mean BOLD signal and hereby neglects the information in the variance of the signal. Further, GLM is a model-based technique which is able to detect only pre-defined effects.

In this paper, we applied a novel nonparametric statistical model to analyse fMRI data from an experiment associated with risky decisions. Our panel dynamic semiparametric factor model (PDSFM) is a model-free, dimension

reduction technique with minimum number of model parameters. DSFM provides a spatial maps common for all studied subjects and time-variant factor loadings which are specific for each individual. Both, spatial maps and factor loadings are very easy to interpret. Statistical inference of the whole high-dimensional data set is based only on the low-dimensional time series (factor loadings).

Applying the PDSFM, we analyzed an fMRI experiment with 17 subjects, each with 722 images of $91 \times 109 \times 91$ voxels. We have identified 20 spatial factors $\widehat{m}_l$, six of them corresponding to mOFC and PC. Other spatial factors were associated with motoric and visualization areas which were connected to the experiment too. Further, we provided the statistical analysis of factor loadins corresponding to the spatial maps in mOFC and PC. We observed that the variability in the responses after the decision stimuli is significantly higher for weakly risk averse individuals then for strongly risk averse individuals. We used the variance of these stimuli responses as input for the classification algorithm. Very high classification rates (100% and 86%) were obtained with the SVM classifier by applying the leave-one-out cross validation algorithm. We classified the risk attitude of the subjects from the low-dimensional representation of the brain activities, without knowing the subject's answers. Herewith we have shown that our PDSFM approach is able to detect the neural representations of risk attitude and to classify the weak and strong averse individuals by their time-dependent factor loadings.

In the literature, the group fMRI analysis is usually carried out by the mixed effects functional model, see Wang (1998); Guo (2002) on the mixed effects model together with Mumford and Poldrack (2007) on the application to fMRI data. Compared to their works, there are several differences in our work. First, their works mainly focus on the univariate (low dimensional) time series, while we focus on the high dimensional time series. For the fMRI data analysis, Mumford and Poldrack (2007) perform the analysis based on some (pre-specified) voxel of special interest, while we try to find both, the temporal dynamics and the regions of special interest (the region w.r.t. risk management in our example) directly based on the high dimensional fMRI time series. Second, as illustrated via a political opinion study discussed in Mumford and Poldrack (2007), the mixed effect model considers the case where subjects participating in the experiment are drawn from several "subgroups" with their own group effect. Contrary, we assume that the subjects participating in our experiment were drawn randomly from the population without considering any special group effects.

Our work, as far as we know, is one of the first works on panel high dimensional time series analysis with multiple subjects. How to extend this to the mixed effects situation is indeed very interesting. One possible way is to add the "group effect" to the time part of Eq.(4), i.e. add an additional term $V_t^T D_l^g$ after $\overline{Z}_{t,l}$ with the "group index" g, design matrices V_t and the coefficient matrix of the unknown "group/fixed" effects D_l^g. However, this is out of the scope of this paper and deserves further research.

(a)

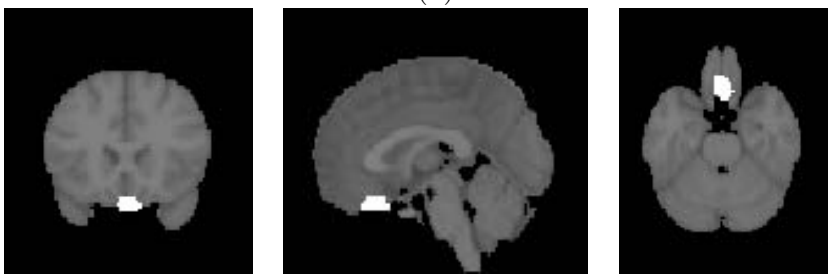

(b)

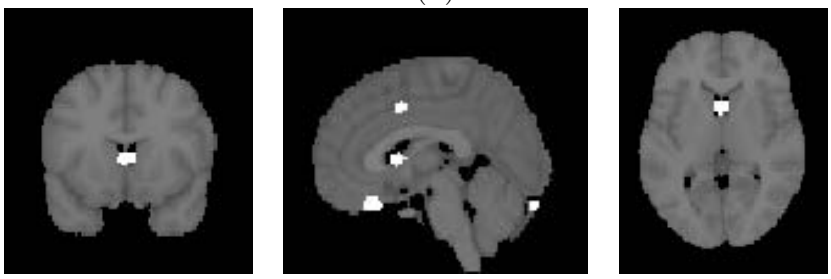

(c)

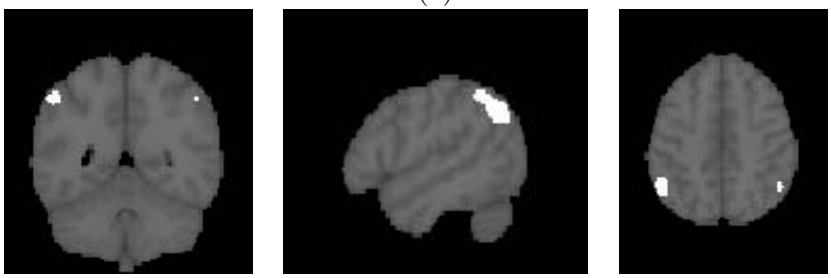

(d)

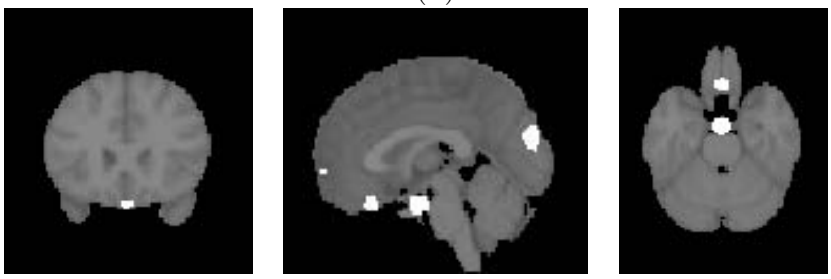

(e)

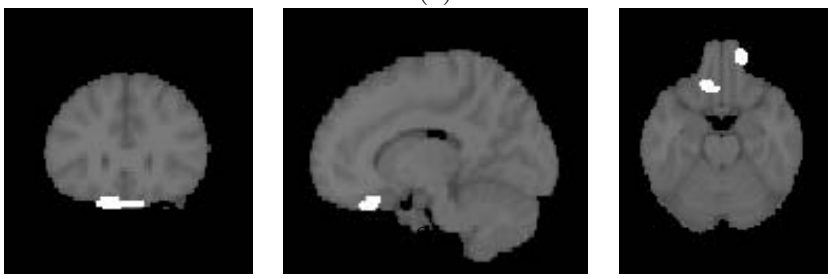

(f)

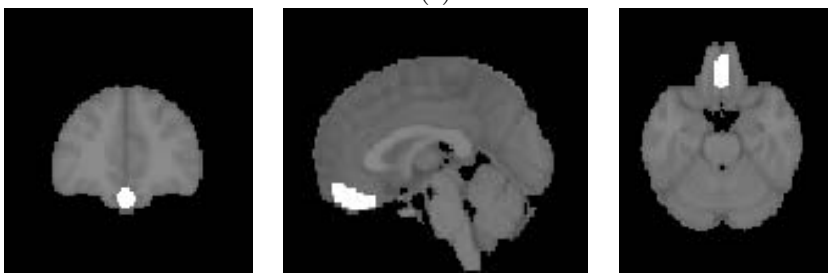

Figure 2: Selected estimated functions $\widehat{m}_l,\ l = 0, \ldots, L$ with $L = 20$. (a) Estimated function $\widehat{m}_5$ with largest values in medial orbitofrontal cortex (mOFC). (b) $\widehat{m}_9$ with largest values in parietal cortex (PC). (c) $\widehat{m}_{12}$ with largest values in mOFC. (d) $\widehat{m}_{16}$ with largest values in mOFC. (e) $\widehat{m}_{17}$ with largest values in mOFC. (f) $\widehat{m}_{18}$ with largest values in mOFC.

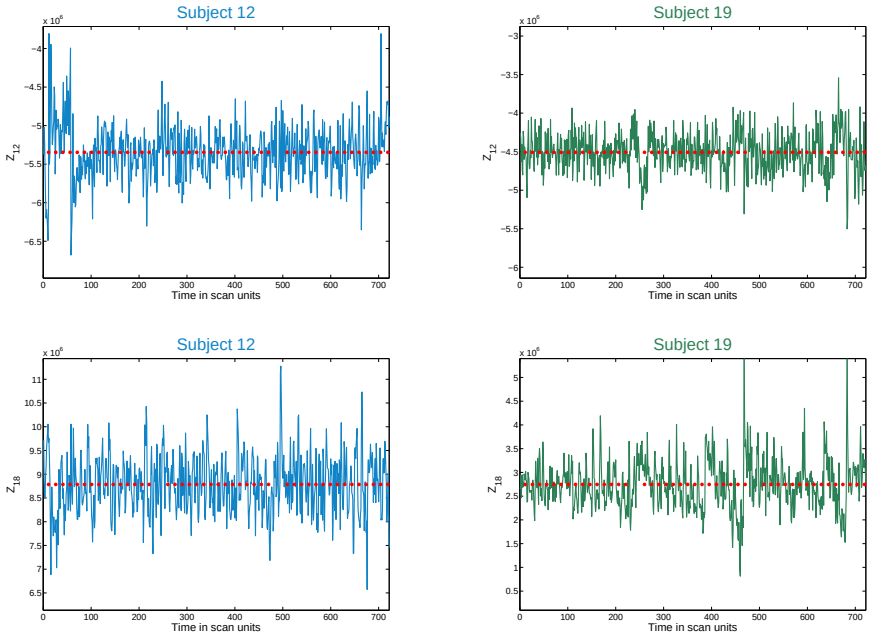

Figure 3: Factors loadings $\widehat{Z}_{t,12}$ (top) and $\widehat{Z}_{t,18}$ (bottom) for subjects 12 (left) and 19 (right) during the whole experiment (722 time points). Red points correspond to the time points of stimuli.

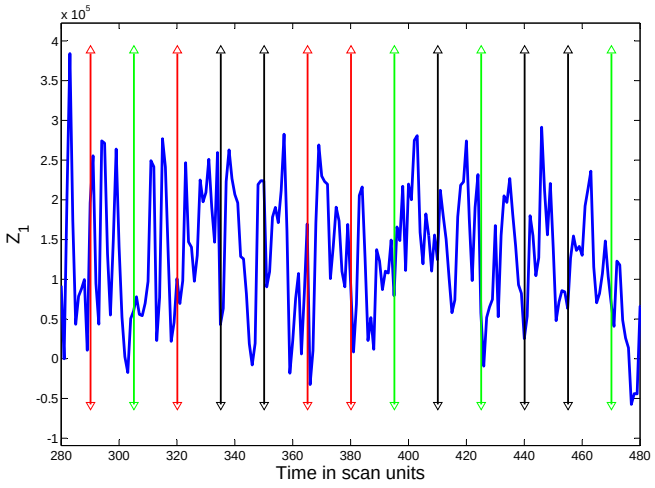

Figure 4: Detailed view of factor loading $\widehat{Z}_{t,1}$ for subjects 12 (blue line) with vertical lines in time points of stimuli of 3 different task: decision (red), subjective expected return (green) and perceived risk (black)

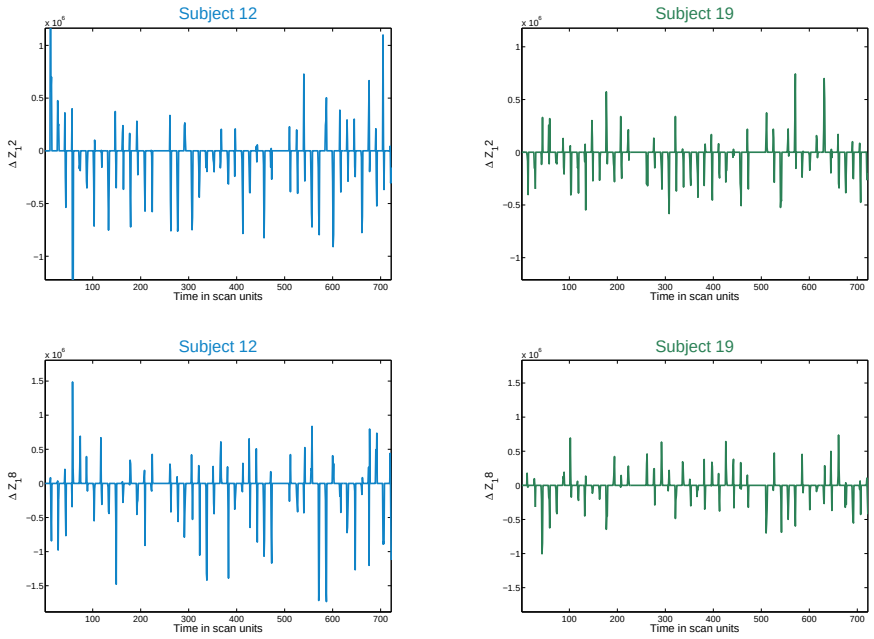

Figure 5: Reaction to stimulus for factors loadings $\widehat{Z}_{t,12}$ (top) and $\widehat{Z}_{t,18}$ (bottom) for subjects 12 (left) and 19 (right) during the whole experiment (45 stimuli).

Appendix A. Plots of average responses to the "Decision under Risk" stimulus

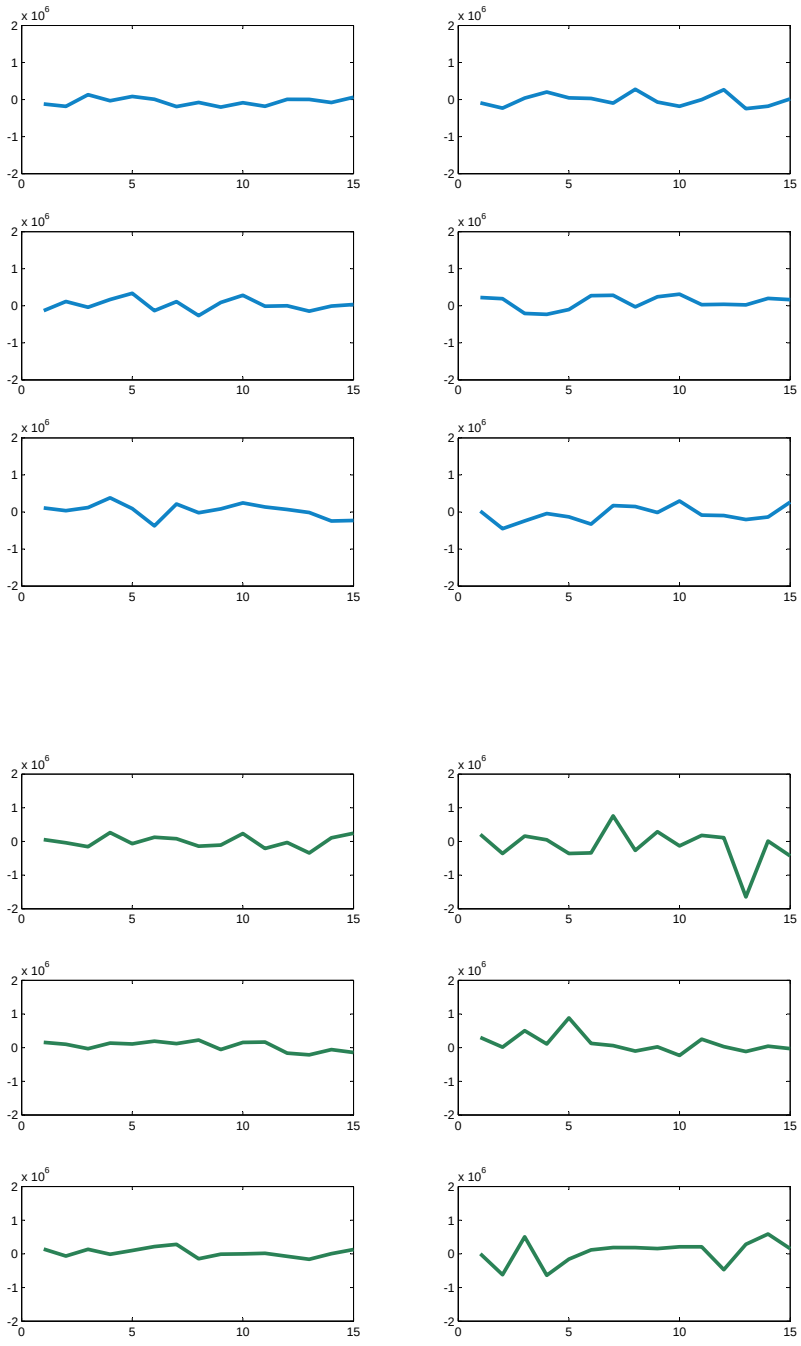

Figure A.6: Average responses to the "Decision under Risk" stimulus in factor loading Z_5 for the weakly risk-averse group (top, blue lines) and strongly risk-averse group (bottom, green lines).

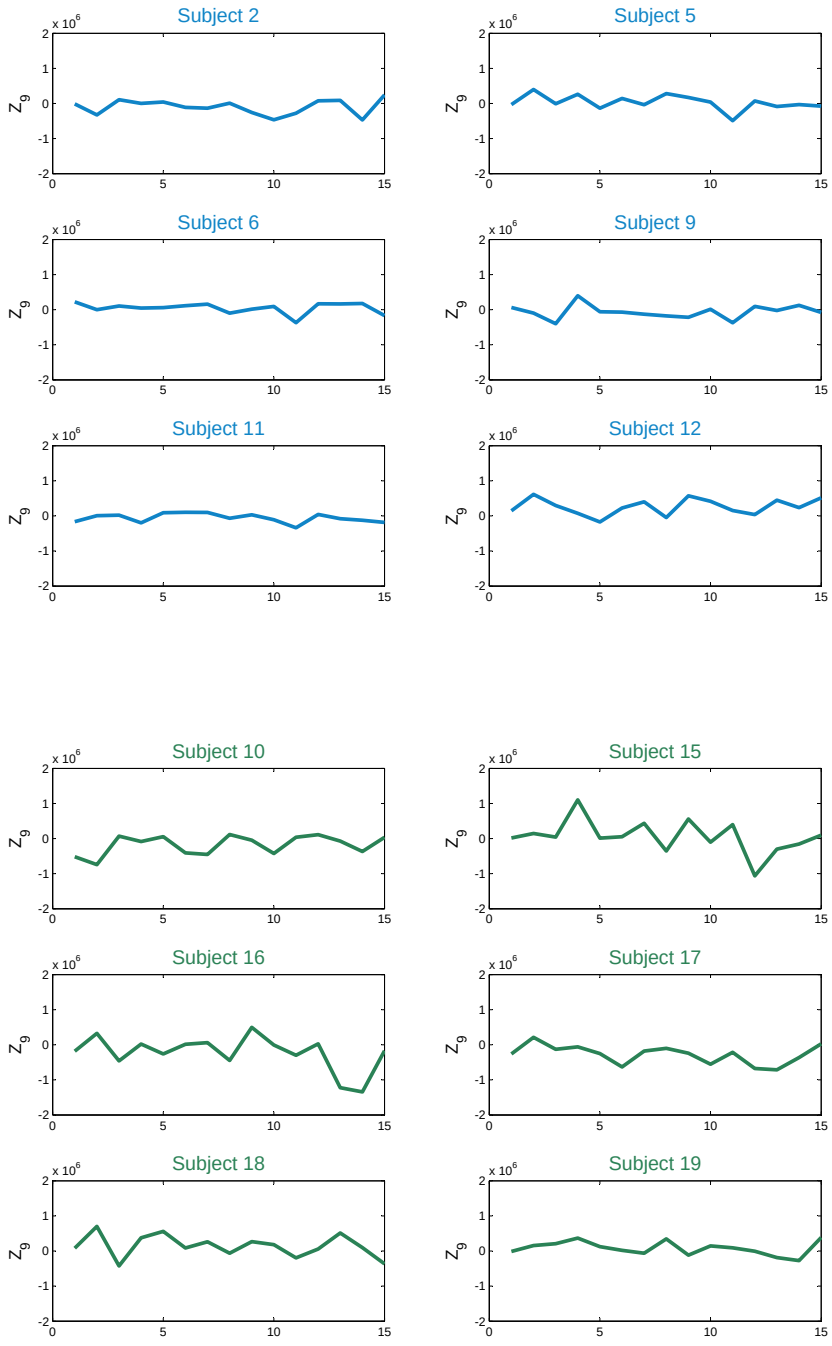

Figure A.7: Average responses to the "Decision under Risk" stimulus in factor loading Z_9 for the weakly risk-averse group (top, blue lines) and strongly risk-averse group (bottom, green lines).

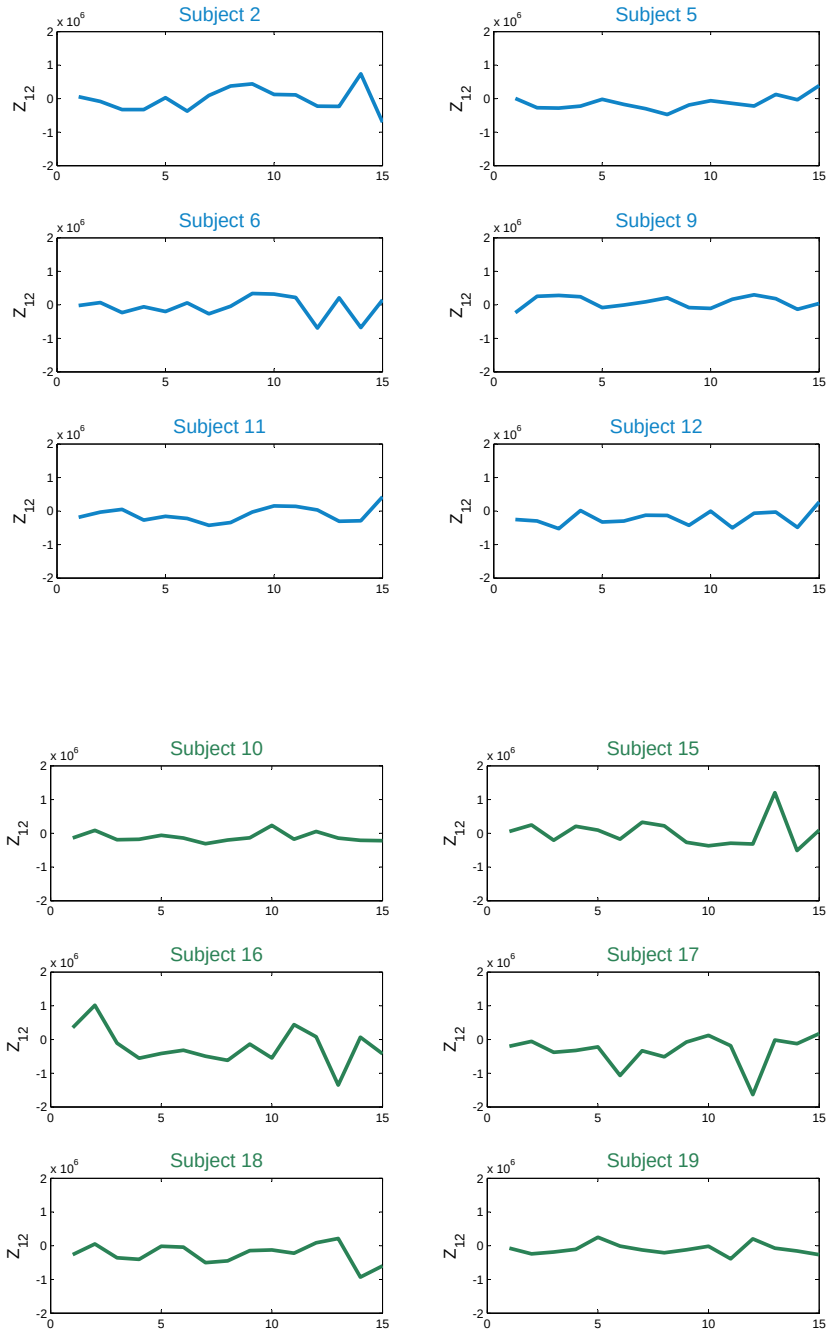

Figure A.8: Average responses to the "Decision under Risk" stimulus in factor loading Z_{12} for the weakly risk-averse group (top, blue lines) and strongly risk-averse group (bottom, green lines).

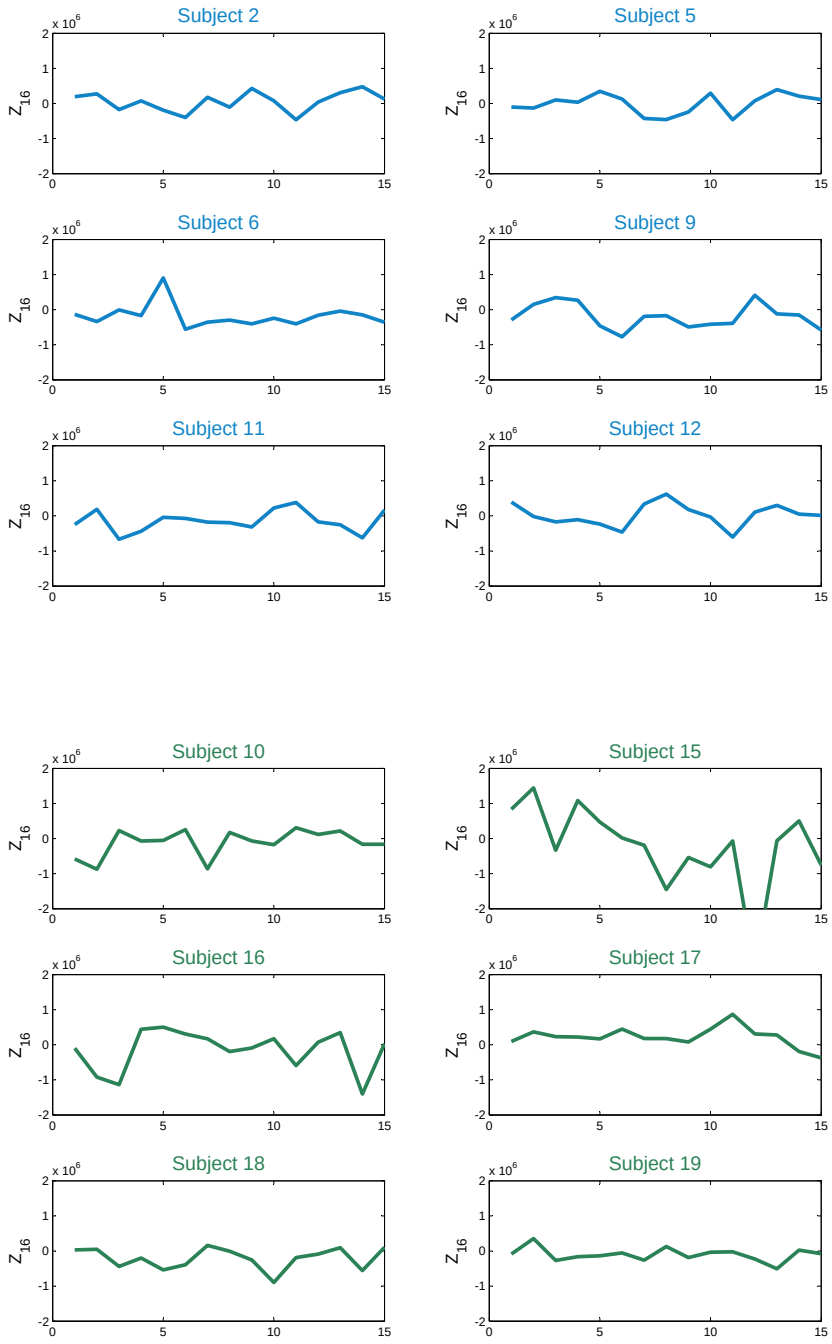

Figure A.9: Average responses to the "Decision under Risk" stimulus in factor loading Z_{16} for the weakly risk-averse group (top, blue lines) and strongly risk-averse group (bottom, green lines).

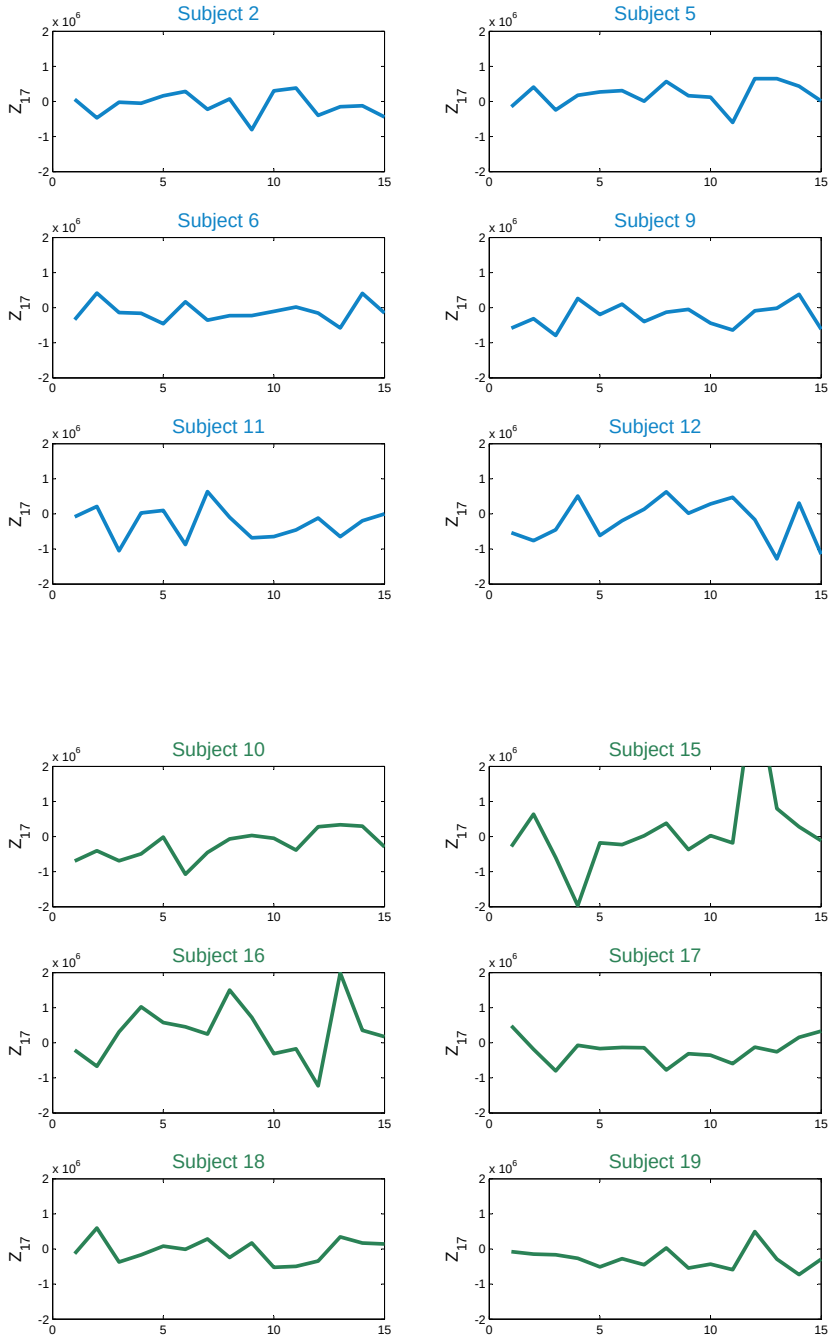

Figure A.10: Average responses to the "Decision under Risk" stimulus in factor loading Z_{17} for subjects 12 (left) and 19 (right).

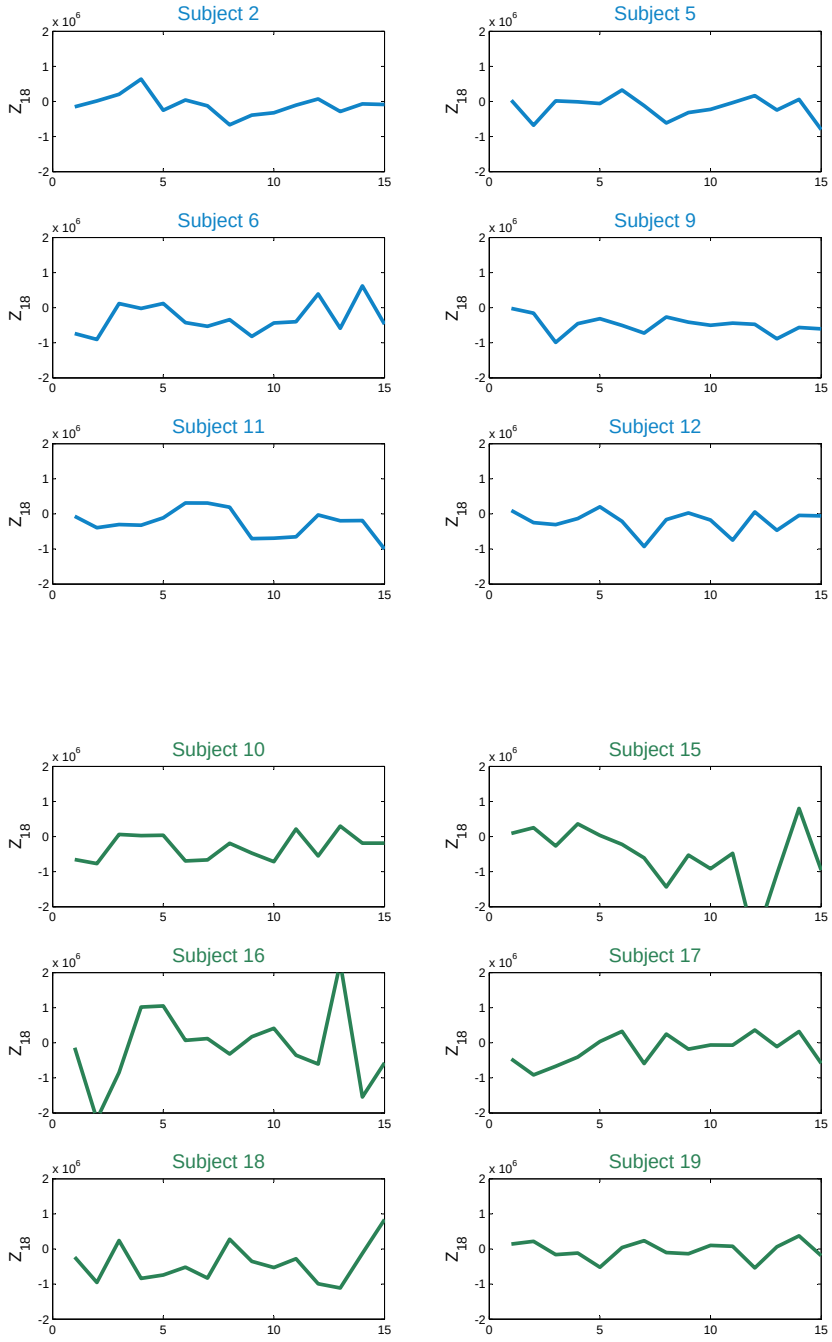

Figure A.11: Average responses to the "Decision under Risk" stimulus in factor loading Z_{18} for subjects 12 (left) and 19 (right).

Appendix B. Residual $\varepsilon^i_{t,j}$ analysis

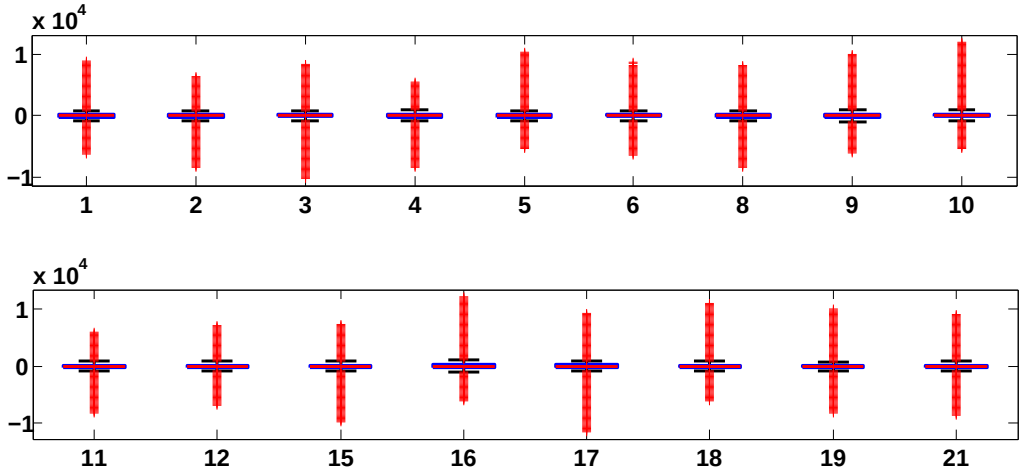

Figure B.12: Boxplots of random subsets (size 3×10^7) from $\varepsilon^i_{t,j}$ (4.3×10^9 points) for all 17 analyzed subjects. Kurtosis exceeds 10

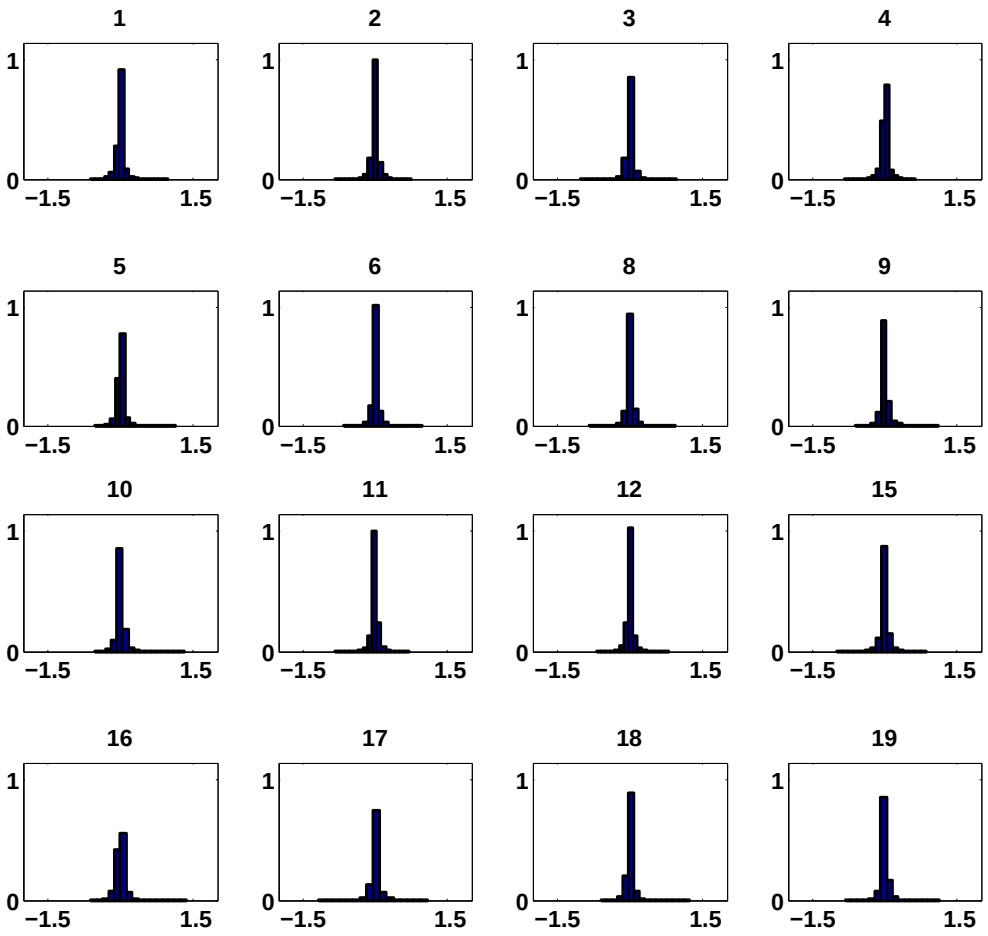

Figure B.13: Histograms of random subsets (size 3×10^7) from $\varepsilon^i_{t,j}$ (4.3×10^9 points) for subjects $i = 1, 2, 3, 4, 5, 6, 8, 9$ (upper panel) and $i = 10, 11, 12, 15, 16, 17, 18, 19$ (lower panel) respectively. Normality hypothesis (**KS test**) for standardized $\varepsilon^i_{t,j}$ rejected for all subjects at significance level 5%

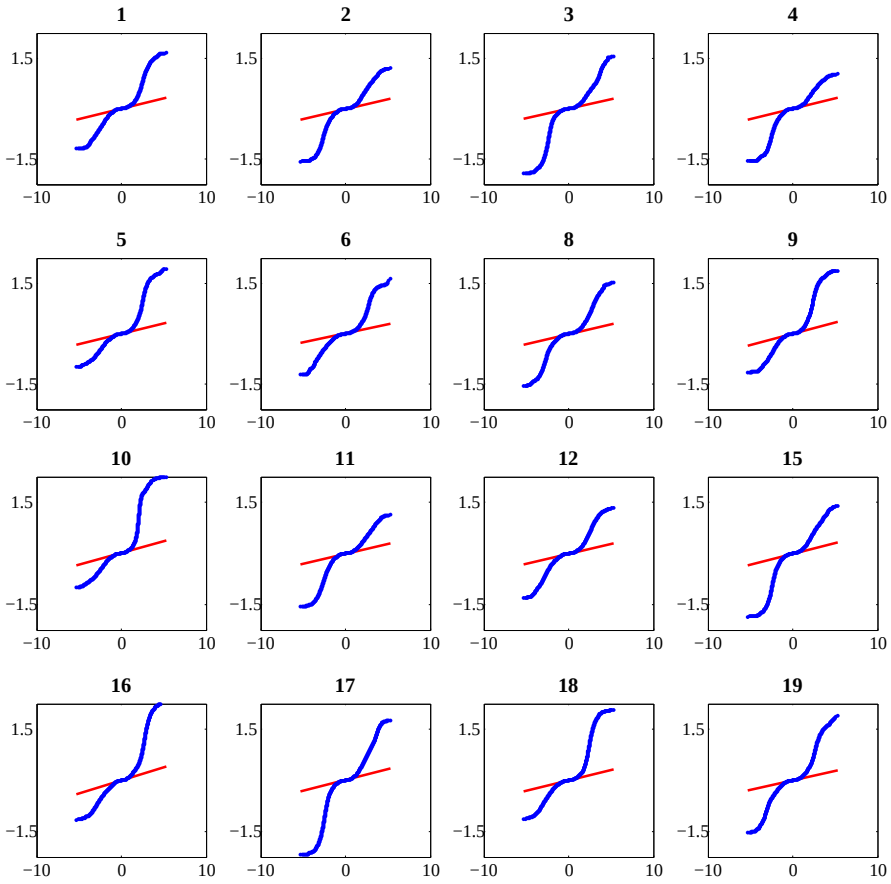

Figure B.14: QQplots of random subsets (size 3×10^7) from $\varepsilon^i_{t,j}$ (4.3×10^9 points) for subjects $i = 1, 2, 3, 4, 5, 6, 8, 9$ (upper panel) and $i = 10, 11, 12, 15, 16, 17, 18, 19$ (lower panel) respectively

References

Beckmann, C., Smith, S., 2005. Tensorial extensions of independent component analysis for multisubject FMRI analysis. Neuroimage 25, 294–311, pARAFAC: R different factor loadings in temporal, spatial and subject domains.

Cortes, C., Vapnik, V., 2005. The nature of statistical learning theory'. Machine Learning 20, 273–297.

Guo, W., 2002. Functional Mixed Effects Models. Biometrics 58, 121128.

Heekeren, H., Marrett, S., Ungerleider, L., 2008. The neural systems that mediate human perceptual decision making. Nat Rev Neurosci 9, 467–479.

Kable, J., Glimcher, P., 2007. The neural correlates of subjective value during intertemporal choice. Nat Neurosci 10, 1625–1633.

Kahneman, D., Tversky, A., 1979. Prospect Theory: An Analysis of Decisison under Risk. Econometrica 47, 263–291.

Klos, A., Weber, E., M., W., 2005. Investment decisions and time horizon: risk perception and risk behavior in repeated gambles. Management Science 51, 1777–1790.

Markowitz, H., 1952. Portfolio Selection. Journal of Finance 7, 77–91.

Mohr, P., Nagel, I., 2010. Variability in brain activity as an individual difference measure in neuroscience? J Neurosci 30, 7755–7757.

Mohr, P. N. C., Biele, G., Krugel, L. K., Li, S.-C., Heekeren, H. R., February 2010. Neural foundations of risk-return trade-off in investment decisions. NeuroImage 49 (3), 2556–2563.
URL `http://dx.doi.org/10.1016/j.neuroimage.2009.10.060`

Mumford, J. A., Poldrack, R. A., 2007. Modeling group fMRI data. Soc. Cogn. Affect. Neurosci. 2, 251257.

Park, B. U., Mammen, E., Wolfgang, H., Borak, S., 2009. Time series modelling with semiparametric factor dynamics. Journal of the American Statistical Association 104 (485), 284–298.
URL http://econpapers.repec.org/RePEc:bes:jnlasa:v:104:i:485:y:2009:p:284-298

Plassmann, H., O'Doherty, J., Rangel, A., 2007. Orbitofrontal cortex encodes willingness to pay in everyday economic transactions. J Neurosci 37, 9984–9988.

Rangel, A., Camerer, C., Montague, P., 2008. A framework for studying the neurobiology of value-based decision making. Nat Rev Neurosci 9, 545–556.

Samanez-Larkin, G., Kuhnen, C., Yoo, D., Knutson, B., 2010. Variability in Nucleus Accumbens Activity Mediates Age-Related Suboptimal Financial Risk Taking. J Neurosci 30, 1426–1434.

Sarin, R., Weber, M., 1993. Risk-value models. European Journal of Operational Research 70, 135–149.

Tobler, P., O'Doherty, J., Dolan, R., Schultz, W., 2007. Reward value coding distinct from risk attitude-related uncertainty coding in human reward systems. J Neurophysiol 97, 1621–1632.

von Neumann, J., Morgenstern, O., 1953. Theory of Games and Economic Behavior. Princton.

Wang, Y., 1998. Mixed effects smoothing spline analysis of variance. Journal of the Royal Statistical Society 60 (Series B), 159–174.

Weber, E., Johnson, E., 2009a. Mindful judgment and decision making. Annual Review of Psychology 60, 5385.

Weber, E., Johnson, E., 2009b. Neuroeconomics. Decision Making and the Brain. Elsevier, London, Ch. Decisions Under Uncertainty: Psychological, Economic, and Neuroeconomic Explanations of Risk Preference, pp. 127–144.